Nonequilibrium gaseous heat transfer in pressure-driven plane Poiseuille flow

Benzi John,* Xiao-Jun Gu, and David R. Emerson
Scientific Computing Department, STFC Daresbury Laboratory, Warrington WA4 4AD, United Kingdom
(Received 31 January 2013; revised manuscript received 19 March 2013; published 29 July 2013)

Nonequilibrium heat and mass transfer in a pressure-driven plane Poiseuille flow is investigated using the direct simulation Monte Carlo method from the early slip to the free molecular regime. Our investigations reveal several nonintuitive, nonequilibrium thermal flow patterns, including expansion cooling near the walls, a nonconstant pressure profile, and counter-gradient heat transfer along the channel center-line. A bimodal trend in the tangential heat flux is found in the slip and the early transition regime. In the upper transition and free molecular regime, the net heat flow in the entire channel is largely unidirectional and in the opposite direction of mass flow. However, in the slip and the early transition regime, a two-way heat flow is observed in the channel as the normal heat flux profile plays a key role in determining the net gaseous heat flow direction. Moreover, the heat flow rate profile exhibits a maximum value at an intermediate value of Knudsen number. The effects of incomplete surface accommodation on nonequilibrium heat flow are also investigated in this work. It is shown that for very low values of the accommodation coefficient, the gaseous heat flow direction is reversed and is consistently in the direction of mass flow.

DOI: 10.1103/PhysRevE.88.013018 PACS number(s): 47.45.−n

I. INTRODUCTION

Fundamental problems in rarefied gas dynamics have received significant attention from the research community over the years. These include the classical problems involving shear-driven, pressure-driven, Fourier, and thermal transpiration flows. Knowledge of the fundamental transport mechanisms in nonequilibrium fluid dynamics not only aids in the development of numerical methods for more complex applications, but is also of practical interest. Nonequilibrium gaseous flows can be accurately represented by the Boltzmann equation. However, it is well known that the complexity of the collision term as well as its high dimensionality precludes its use for many real applications. As a consequence, a wide range of macroscopic models have been developed over the years [1–4], and while they provide computational efficiency, none can claim accuracy and reliability for the entire range of Knudsen numbers. The most notable macroscopic methods are the well known slip-based models, the method of moments [5–7], and the Burnett equations [8,9]. Methods based on the linearized Boltzmann equation have been employed by many researchers [10–12] for nonequilibrium flows, including for the case of a very high Knudsen number with good success. However, they are only suitable for applications involving very low flow-gradients, so that the Boltzmann equation can be linearized around an equilibrium state at rest. This limits its practical use beyond certain ideal flow situations. Alternately, the direct simulation Monte Carlo method (DSMC) [13] can be employed, which is widely accepted as the most reliable method for nonequilibrium gaseous flow simulations. DSMC is based on the discrete molecular nature of the gas and essentially capturing the physics of a dilute gas governed by the Boltzmann equation.

Numerous works have been reported that deal with Couette, Poiseuille, and Rayleigh flows [14–25]; however, very few give significant attention to gaseous heat transfer. Heat transfer calculations under nonequilibrium flow conditions is challenging as it depends upon a combination of various factors such as compressibility, viscous dissipation, expansion cooling, thermal creep, etc. Moreover, from a kinetic point of view, temperature and heat flux are higher-order moments, and hence, Navier-Stokes-Fourier (NSF) equation-based methods often fail to predict these quantities accurately. Several anomalous flow features have been reported in the literature that NSF-based methods cannot capture, even qualitatively, especially with respect to thermal aspects. An example is the bimodal temperature distribution in force-driven Poiseuille flows [17,18], which is accurately predicted by DSMC and higher-order moment methods, but not by the NSF models. In the case of planar Couette flow, there exists a nonzero tangential heat flux [6] that is not predicted by the NSF equations. Recently, the authors in their work revealed some interesting counter-gradient heat flux thermal patterns in a lid-driven cavity [21,22], i.e., heat flows from a cold region to a hot region, which the slip and temperature jump corrected NSF equations cannot predict even in the early slip regime. A brief comparison of nonequilibrium heat transfer between acceleration and pressure-driven Poiseuille flows were recently reported by the authors [23]. Although only a limited range of Knudsen numbers was considered for the pressure-driven Poiseuille flow, it was clear that further work was needed to fully understand the nonintuitive features being observed.

In this work, we investigate the nonequilibrium gaseous heat transfer characteristic details of pressure-driven plane Poiseuille flow using the DSMC method. A substantial amount of work has been reported in the literature related to plane Poiseuille flows, both for the pressure-driven and acceleration-driven cases. Acceleration-driven Poiseuille flow has been studied by Aoki *et al.* [20] with the aid of the linearized Boltzmann equations and by Uribe and Garcia [19] using the Burnett equations and DSMC. A numerical analysis of pressure-driven Poiseuille flow on the basis of the linearized Boltzmann equation for hard-sphere molecules has been

*benzi.john@stfc.ac.uk

carried out by Ohwada *et al*. [26]. In Ohwada's study, heat flow was considered and tangential heat flux profiles were shown for three cases of modified Knudsen number k; i.e., $k = 0.1$, 1, and 10, where $k = (\sqrt{\pi}/2)\mathrm{Kn}$ and $\mathrm{Kn} = \lambda/H$, λ being the mean free path and H being the channel height. It was inferred from the tangential heat flux profiles that at $k = 0.1$, the heat flows in the opposite direction to the mass flow at the center of the channel but close to the wall; heat flow was found to be in the same direction as the mass flow. It was also noted that at higher Knudsen numbers the heat flow was always in the opposite direction to the mass flow. However, in their analysis, the normal heat flux profiles were not considered. This is important as the net heat flow direction is determined by both tangential and normal heat fluxes. Also, gaseous heat flow in the slip and near continuum regime was not studied in their work. Neither were the effects of pressure ratio on the heat flux profiles studied. In a separate study by Zheng *et al*. [27], comparisons between kinetic theory and hydrodynamics for Poiseuille flow for the case of force-driven and pressure-driven Poiseuille flows were made. In their work, comparisons of velocity, temperature, and pressure profiles computed by DSMC and NSF methods at $\mathrm{Kn} = 0.1$ were made. Varoutis *et al*. [28] recently studied rarefied gas flow through channels of finite length at various pressure ratios. Flow rates and other gaseous flow characteristics were studied for a wide range of Knudsen numbers. However, detailed studies of nonequilibrium gaseous heat transfer were not reported. Recent advances in MEMS fabrication technology mean that it is now possible to have extremely smooth and clean surfaces, implying that the accommodation coefficient could be much less than unity. Incomplete surface accommodation is known to result in higher mass flow rates in Poiseuille flows. However, the effects of partial surface accommodation on nonequilibrium heat transfer in the channel are not well known and such studies are in paucity in the literature. Accurate simulation of nonequilibrium heat transfer can give critical information to designers toward understanding the thermal characteristics in micro- and nanochannels. Hence, the objective of this study is to obtain a more complete understanding of nonequilibrium heat transfer in Poiseuille flow over a wide range of flow rarefaction (i.e., from the early slip regime through to the free molecular regime) and also to study the effects of incomplete surface accommodation. In particular, the emphasis is on understanding detailed thermal characteristics under nonequilibrium flow conditions.

II. NUMERICAL RESULTS AND DISCUSSION

To ensure consistency for all cases, the plane-Poiseuille geometric configuration is kept fixed. The aspect ratio, L/H considered here is 5, where L is the channel length and H is the channel height. The flow is driven by a pressure gradient that is maintained by imposing a pressure ratio between the channel inlet and outlet. The wall temperature and the inlet temperature are set to the reference temperature, i.e., $T_0 = T_i = T_w = 273$ K. Numerical simulations have been carried out for a wide range of Knudsen numbers from the early slip regime through to the free molecular regime. The Knudsen number variation is achieved by varying the density conditions at the outflow, i.e., the outlet pressure P_o, at which the simulation is carried out varies for each Kn. Only selected results will be shown here, i.e., $\mathrm{Kn} = 0.025$, 0.05, 0.1, 0.5, 1, and 10.

All the simulations in the present study are performed with a validated parallel DSMC code that has been successfully employed for flow simulations in various micro-geometries [21,22,30,32,33]. The variable hard sphere (VHS) collision model [13] has been used with a monatomic molecule of mass $m = 6.63 \times 10^{-26}$ kg, and reference particle diameter of $d = 4.17 \times 10^{-10}$ m. The particle-wall interactions follow the Maxwell model. Pressure boundary conditions [29–33] are imposed at the inflow and outflow, where the pressure P_i and temperature T_i at the inflow, and the pressure P_o at the outflow are fixed. The general guidelines that need to be followed for an accurate DSMC simulation, with respect to the cell size, time step, and particle number are well documented in the literature [34–36]. In the present work, these guidelines have been rigorously followed to ensure the accuracy of the computed flow results. The flow variables are derived as time-averages during the sampling phase, which in this study have been carried out over a period of several million time steps after the system has reached a steady state.

The variation of computed tangential and normal heat flux profiles, q_x and q_y, along a vertical line located at a distance of $2L/3$ from the entrance of the channel is shown in Fig. 1 and Fig. 2. The heat flux profiles in these plots are nondimensionalized with respect to the parameter, q_0, where $q_0 = \mu R T_0/H$, in which μ is the viscosity of the gas based on the reference temperature and R is the gas constant. Comparisons are shown at two pressure ratios, i.e., $P_i/P_o = 2$ and $P_i/P_o = 1.5$. Many of the variations observed in these plots are subtle and could be indistinguishable due to the statistical nature of the DSMC data. Hence, for the sake of clarity, the heat flux profiles shown in Figs. 1 and 2 are polynomial fitted. The heat flux profiles indicate several interesting trends in the heat flow pattern in the channel. It is interesting to note that there exists a definite nonzero tangential heat flux for the case of nonequilibrium Poiseuille flow. The tangential heat flow in the channel-center region has been identified as a higher-order rarefaction effect [25,26] as a result of the pressure gradient, whereas near the walls in the early transition regime the heat flow induced by the Knudsen layer dominates the heat flow resulting from the pressure gradient. From the heat flux plots it is observed that the values decrease with an increase in flow rarefaction. This can be attributed to the fact that collision frequency significantly reduces with an increase in flow rarefaction. More interestingly, the tangential heat flux profiles reveal a bimodal shape with a dip in the center in the slip and early transition regimes. The bimodal shape, however, diminishes with increasing Kn as the profiles follow a parabolic pattern in the upper transition regime and beyond. A comparison of q_x profiles between the two pressure ratios considered clearly indicates that the bimodal trend is more pronounced at a higher pressure ratio and also in the early slip regime close to continuum. This trend suggests that for extremely low pressure ratios, the bimodal trend in

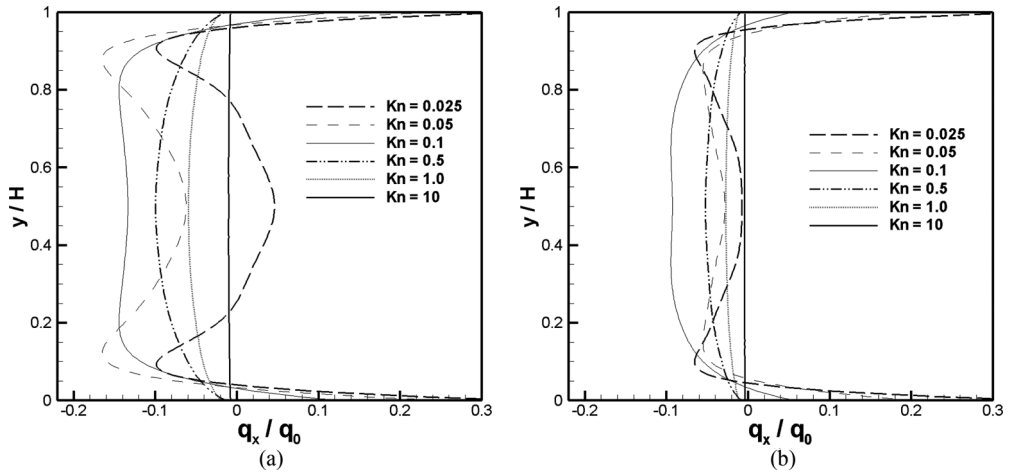

FIG. 1. Variation of computed tangential heat flux profiles, q_x at different pressure ratios (a) $P_i/P_o = 2$ and (b) $P_i/P_o = 1.5$, plotted as a function of Kn at $x/L = 2/3$.

the tangential heat flux will be completely absent even at a relatively low Kn. This is perhaps the reason why no bimodal trend in the q_x profiles were discovered in the work by Ohwada *et al*. [26], as they only considered extremely low pressure ratios for the linearized Boltzmann equation to be valid. The computed heat flux profiles in this work show that $q_x > 0$ near the walls, from the slip to the early transition regime, while in the rest of the channel it is negative. In Ohwada's work, it was pointed out based on the tangential heat flux profile that at Kn $\sim$ 0.11 (in the early transition regime), the heat flow along the centerline is in the opposite direction of mass flow, whereas along the walls the heat flow will be in the same direction as mass flow. Although this is generally true, the DSMC results in this study indicate that it is also dependent on the pressure ratio. The computed q_x profiles show that heat flow need not be always in the opposite direction as that of mass flow (i.e., $q_x < 0$) along the center of the channel, as it is found that $q_x > 0$ along the center-line at $P_i/P_o = 2$ and at Kn $= 0.025$ (i.e., in general, the early slip regime at high pressure ratios). The normal heat flux profiles were not considered in Ohwada's work, but our study shows that the normal heat flux plays a significant role, especially in regions near the walls in the slip and early transition regimes, as it affects the net gaseous heat flow direction in the channel dramatically.

The predicted normal heat flux, q_y profiles in Fig. 2 show a sinusoidal pattern. For all cases of Kn considered, the magnitude of q_y is maximum in regions close to the wall, whereas along the center of the channel, $q_y = 0$. This indicates that close to the walls, two-dimensional effects are important in determining the net heat flow direction for all the cases of Kn, whereas along the center of the channel the heat flow will be unidirectional as it is solely determined by the tangential heat flux. In particular, at a relatively low Kn (i.e., in the early slip regime), the magnitude of q_y is much higher compared to that of q_x, which means that in this regime the heat flow in almost the entire channel will be largely in a direction normal to that of the mass flow direction (i.e. in the y-direction), except along the center of the channel where heat flow will be always in the x direction. The significance of the normal heat flux profiles diminishes with increasing Kn. Hence, in the upper transition regime and in the free

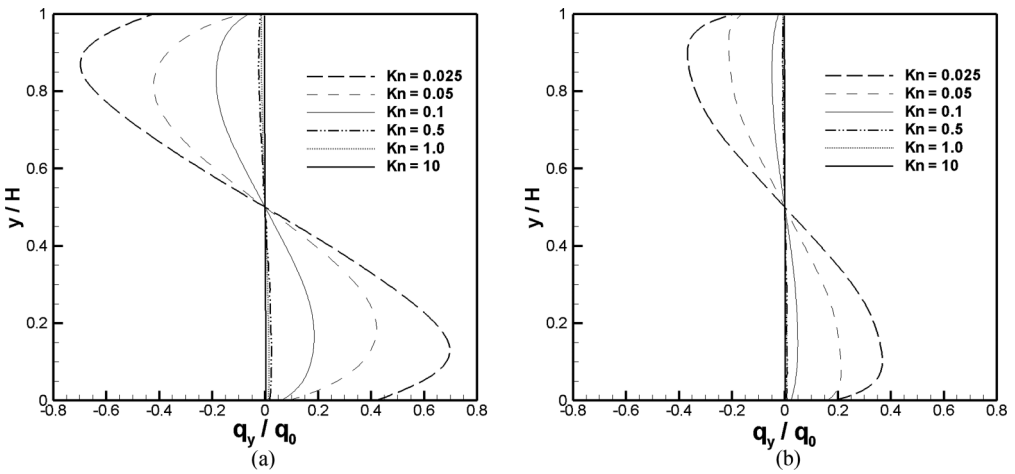

FIG. 2. Variation of normal heat flux profiles, q_y computed at different pressure ratios (a) $P_i/P_o = 2$ and (b) $P_i/P_o = 1.5$, plotted as a function of Kn at $x/L = 2/3$.

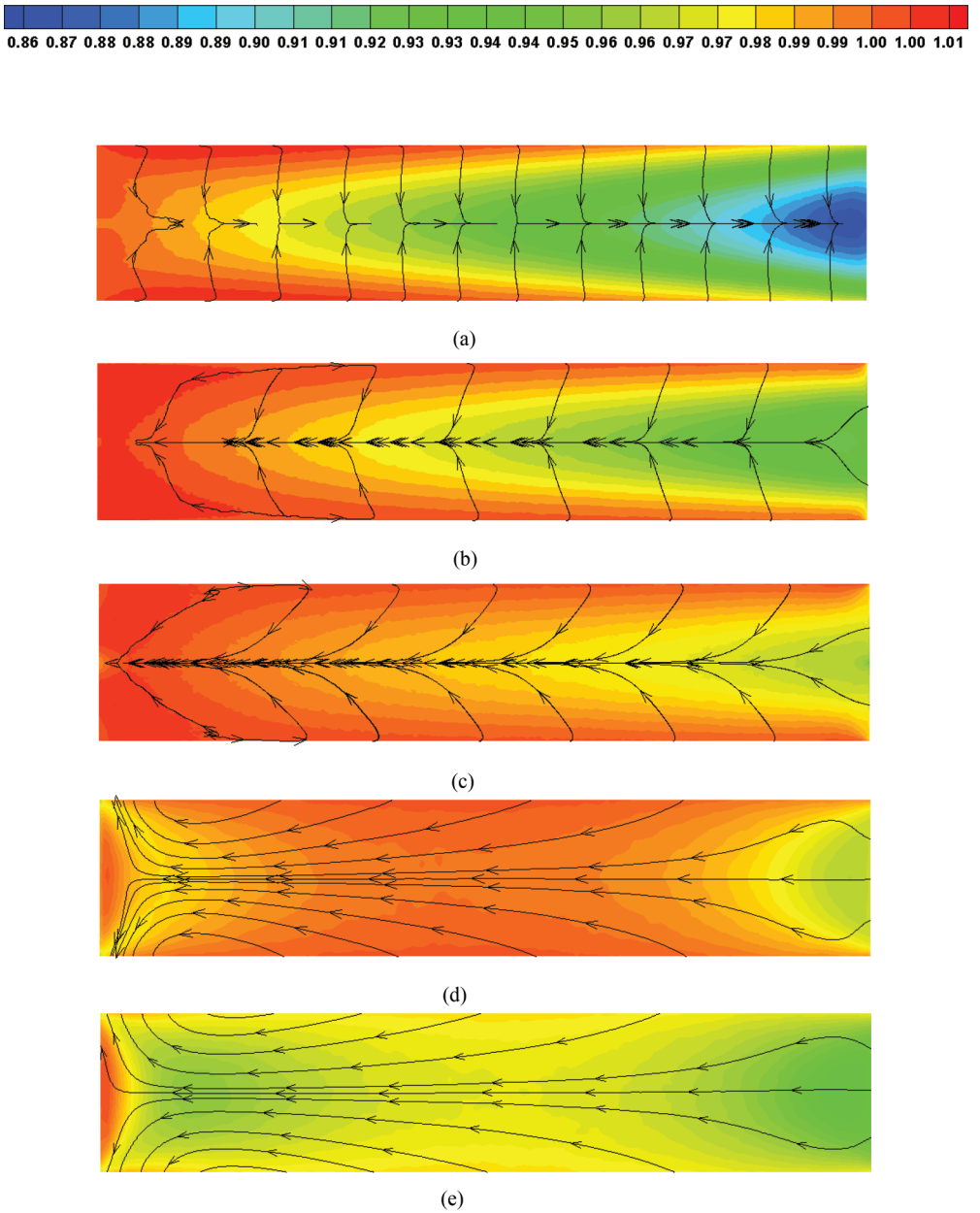

FIG. 3. (Color online) Comparison of heat flux stream traces overlaid on temperature (T/T_0) contours computed at $P_i/P_o = 2$ for different cases of Kn (a) Kn = 0.025, (b) Kn = 0.05, (c) Kn = 0.1, (d) Kn = 1.0, and (e) Kn = 10.

molecular regime, heat flow will be consistently unidirectional (in the opposite direction of mass flow) in almost the entirety of the channel. These thermal patterns and the net gaseous heat transfer direction in the channel can be clearly visualized from Fig. 3, which shows plots of two-dimensional heat flux stream traces overlaid on temperature contours at selected values of Kn. Many nonequilibrium heat flow phenomena can be seen from the thermal patterns. From the temperature contours it is observed that there is a significant drop in temperature toward the channel outlet. This can be attributed to the pressure drop and corresponding flow expansion at the outlet. Interestingly, at a higher Kn, a temperature drop is observed in regions near the channel entrance in addition to that observed near the outlet, as the temperature jump phenomenon increases with flow rarefaction. As expected, the temperature variations in the channel are minimal in the upper transition regime and the free molecular regime, when compared to those at lower Kn. From the heat flux streamlines, a two-way heat flow pattern is observed in the slip regime, i.e., heat flow along the channel-center is in the x direction, whereas in the rest of the channel it is in a direction normal to that for the mass flow. It is noteworthy that at Kn = 0.1, net heat flow in almost the entirety of the channel is largely in the opposite direction of mass flow despite the positive q_x profiles near the walls. We further note that the gaseous heat flow direction along the channel-center is mostly from a cold region to a hot region. This is a counter-gradient heat transfer pattern that the Navier-Stokes-Fourier equations cannot predict. The temperature profiles along a vertical line located at a distance of $2L/3$ from the entrance of the channel computed at $P_i/P_o = 2$

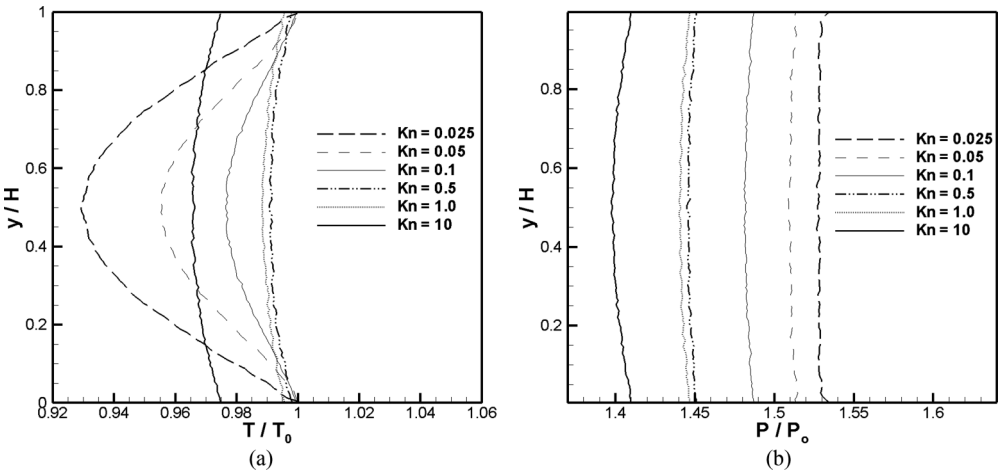

FIG. 4. Predicted (a) temperature and (b) pressure profiles computed at $P_i/P_o = 2$, plotted as a function of Kn at $x/L = 2/3$.

are shown in Fig. 4(a). It is noted that along the walls, the gas temperature is less than the wall temperature, i.e.,$T < T_w$ for all the cases of Kn considered. For Poiseuille flow, the pressure drops along the length of the channel. Near the walls this leads to an expansion cooling phenomenon (i.e., $T < T_w$), which results in heat transfer from the wall to the gas. The expansion cooling phenomenon near the walls increases with Kn.

Comparison of pressure profiles along the vertical line is shown in Fig. 4(b). In the plots, the pressure values are normalized by the reference pressure P_o (i.e., the outlet pressure at each Kn) for each case. The pressure variations are dependent on the variations in temperature and density in the channel. For Poiseuille flow in the continuum regime, a constant pressure profile with no pressure gradient in the normal direction is expected. At Kn $= 0.025$, the pressure profile in the normal direction is almost a straight line. However, for Kn $\geqslant 0.05$, nonconstant pressure profiles are observed with a minimum located at the center of the channel. This trend in the pressure profile becomes more apparent with increasing Kn.

The computed nondimensional heat flow rate, Q, plotted as a function of Knudsen number is shown in Fig. 5, where Q is calculated as $Q = \int_0^H q_x dy/\mu R T_0$. We note that $Q > 0$ only for the case of Kn $= 0.025$ at $P_i/P_o = 2$. This can be attributed to the bimodal tangential heat flux profile and the fact that $q_x > 0$ along the channel center-line for this particular case. For all other cases considered, $Q < 0$ as the heat flow is mostly in the opposite direction of mass flow. From the heat flow rate profile, it is noted that there exists a minimal value of Q at an intermediate value of Knudsen number, i.e., at about Kn $= 0.1$, for both cases of pressure ratios considered. It is noteworthy that when considered in terms of magnitude, it is actually a heat flow maximum that is observed in the case of pressure-driven Poiseuille flow. To give an idea of the range of flow conditions for various values of Kn adopted in the present study, we note that the maximum flow velocity range from about 260 m/s for Kn $=$ 0.025 to about 60 m/s for Kn $= 10$. The maximum density for Kn $= 0.025$ is about 3.6 kg/m^{3}while that at Kn $= 10$ is 0.009 kg/m^3.

A. Impact of incomplete surface accommodation

It is well known that incomplete surface accommodation increases the flow velocity and mass flow rate in Poiseuille flows [25,26,37]. In the present work these aspects are not discussed and instead focus is given toward understanding the thermal characteristics, which are investigated as a function of the accommodation coefficient, α. Temperature and tangential heat flux profile variations computed for $P_i/P_o = 2$ at Kn $= 1$ are shown in Fig. 6, whereas Fig. 7 shows the corresponding plots of heat flux stream traces overlaid on temperature contours as a function of α. The heat flux profiles and streamlines reveal interesting heat flow patterns in the channel. Decreasing values of α lead to a weaker interaction of gas molecules with the wall and a higher flow velocity, which results in a significant drop in temperature toward the channel outlet for low values of α. From the tangential heat flux profiles it can be seen that the magnitude of the heat flux values, in general, reduces with a decrease in α. The variations in q_x

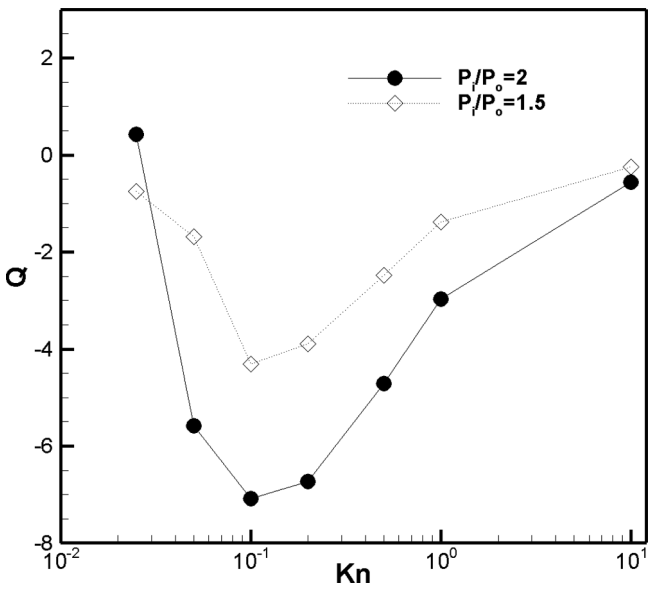

FIG. 5. Predicted heat flow rate plotted as a function of Kn for the pressure-driven Poiseuille flow.

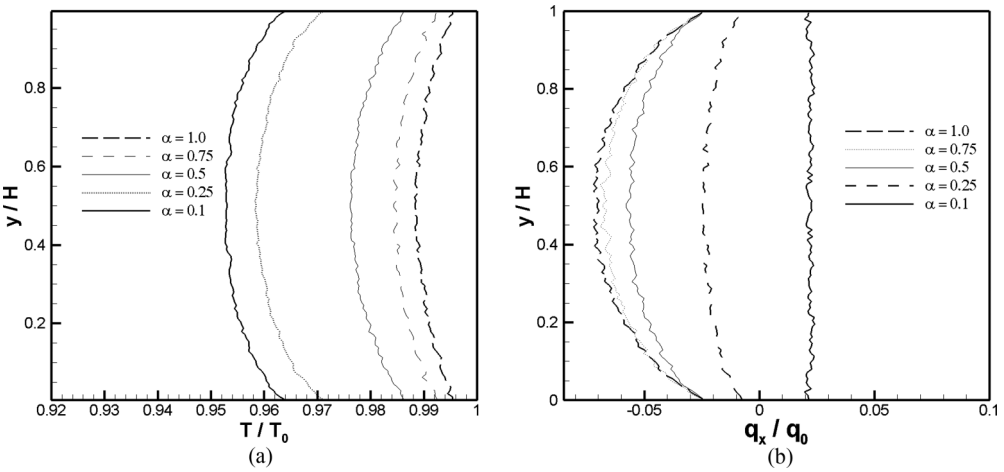

FIG. 6. Predicted (a) temperature and (b) tangential heat flux profiles plotted as a function of α at $x/L = 2/3$.

across the channel are minimal at low values of α. More importantly, the gaseous heat transfer direction is found to be significantly affected by these changes. When $\alpha < 0.5$, the number of molecules contributing to adiabatic exchange with the walls outweigh those contributing to diffuse wall reflections. As a result, when $\alpha < 0.5$, the heat transfer mechanism changes as the channel temperature patterns and tangential heat flux profile characteristics change significantly.

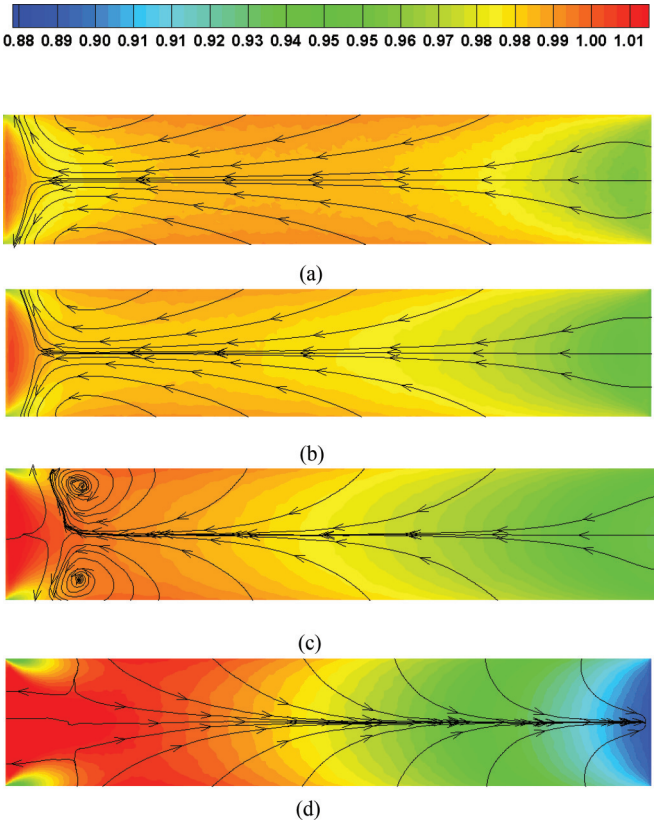

FIG. 7. (Color online) Comparison of heat flux stream traces overlaid on temperature (T/T_0) contours computed at Kn = 1 and $P_i/P_o = 2$ for different cases of α (a) $\alpha = 0.75$, (b) $\alpha = 0.5$, (c) $\alpha = 0.25$, and (d) $\alpha = 0.1$.

For very low values of α, the heat flux values change in sign as shown in Fig. 6(b). In particular, when $\alpha = 0.1$, a tangential heat flow is induced by the large temperature gradient, which dominates that induced by the pressure gradient. These trends can be clearly seen from the heat flux stream line plots in the channel, where at $\alpha = 0.1$, the gaseous heat transfer direction reverses and becomes consistently in the mass flow direction, unlike for the cases with higher values of α, where the heat flow is in the opposite direction of mass flow.

B. Additional comments

It is to be noted that extremely high aspect ratios would be ideal to minimize the entrance and exit effects and to ensure fully developed flow conditions. However, the DSMC method becomes computationally prohibitive when the flow is close to the continuum regime, which means that very high aspect ratios cannot be considered for very low values of Kn. Simulations at high Kn, however, could be done for very large aspect ratios. We carried out several DSMC simulations to verify the generality of the results shown in the present work, i.e., for smaller and larger aspect ratios than $L/H = 5$ at a relatively higher Kn. Our investigations yielded essentially very similar heat transfer characteristics. We show thermal characteristics for two selected cases at Kn = 10 with very high aspect ratios of $L/H = 15$ and $L/H = 20$ in Fig. 8. The pressure ratios considered for these two cases are 6 and 8, respectively, so as to keep the same pressure gradient as

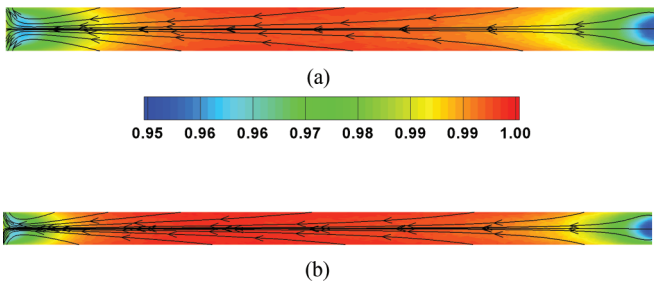

FIG. 8. (Color online) Comparison of heat flux stream traces overlaid on temperature (T/T_0) contours computed at Kn = 10 for (a) $L/H = 15$, $P_i/P_o = 6$ and (b) $L/H = 20$, $P_i/P_o = 8$.

that considered in the paper for $L/H = 5$ and $P_i/P_o = 2$. For both cases considered, the temperature profiles and heat flow direction are very similar and consistent with the results for $L/H = 5$. This proves that at high Kn, regardless of the pressure ratio and aspect ratio considered, the thermal pattern in the bulk of flow remains unaffected and the heat flow in the channel is consistently in the opposite direction of mass flow. The other noteworthy aspect for discussion is the boundary condition at the inflow and outflow. Authors are of the view that DSMC boundary conditions for confined microflows in the present work as well as in many previous works by other researchers are not exact, unlike those for external supersonic flows. The main reasons for this are the relatively low flow speeds, influence of the walls, and limitations in obtaining analytical expressions relating nonequilibrium temperature, heat flux, and velocity, while at the same time embodying the pressure information to be fixed at the inflow and outflow boundaries. However, in practice, the existing schemes work very well and are validated for a wide range of microflow conditions. Any numerical error is expected to be small and limited to very small regions near the inflow and outflow. It is to be noted that all basic tangential heat flux trends reported in Ohwada's work [12] have been reproduced by our DSMC simulations in this work.

III. CONCLUSIONS

Gaseous flow and heat transfer in a pressure-driven plane Poiseuille flow is investigated using the direct simulation Monte Carlo method from the early slip regime to the free molecular regime. Several nonintuitive thermal flow patterns have been observed from our investigations. An expansion cooling phenomenon near the walls and a nonconstant pressure profile in the normal direction are observed from the computed results, both of which become more pronounced with increase in flow rarefaction. The expansion cooling phenomenon results in heat transfer from the wall to the gas. A bimodal trend in the tangential heat flux profiles is revealed in the slip and early transition regime at relatively high pressure ratios. The bimodal trend, however, is absent in the upper transition and free molecular regimes and becomes less pronounced for lower pressure ratios. At a high Knudsen number, the net heat flow in the entire channel is largely unidirectional and in the opposite direction of mass flow. In the slip regime, however, a two-way heat flow pattern is observed, as the normal heat flux values become significant, especially in regions close to the walls. Our computations also show that in the early slip regime, the heat flow direction along the channel center-line is dependent on the pressure ratio considered. In addition, the nondimensional heat flow rate profile exhibits a heat flow maximum at an intermediate value of Knudsen number. The effect of incomplete surface accommodation on nonequilibrium heat flow is also considered in this study. Heat flux variations in the channel are minimal for low values of the accommodation coefficient, as the degree of wall thermal insulation increases. For very low values of the accommodation coefficient, the gaseous heat flow direction reverses completely and is consistently in the direction of mass flow.

ACKNOWLEDGMENTS

The authors thank the Engineering and Physical Sciences Research Council (EPSRC) for its support of Collaborative Computational Project 12 (CCP12).

[1] C. Cercignani, *The Boltzmann Equation and Its Applications* (Springer, New York, 1988).
[2] M. Gad-el-Hak, ASME Trans. J. Fluids Eng. **121**, 5 (1999).
[3] S. Chapman and T. G. Cowling, *The Mathematical Theory of Nonuniform Gases* (Cambridge University Press, Cambridge, 1970).
[4] H. Grad, Commun. Pure Appl. Math. **2**, 331 (1949).
[5] H. Struchtrup, *Macroscopic Transport Equations for Rarefied Gas Flows* (Springer-Verlag, Berlin, 2005).
[6] X. J. Gu and D. R. Emerson, J. Fluid Mech. **636**, 177 (2009).
[7] X. J. Gu and D. R. Emerson, J. Comput. Phys. **225**, 263 (2007).
[8] L. S. Garcia-Colin, R. M. Velasco and F. J. Uribe, Phys. Rep. **465**, 149 (2008).
[9] A. V. Bobylev, Sov. Phys. Dokl. **27**, 29 (1982).
[10] Y. Sone, T. Ohwada, and K. Aoki, Phys. Fluids A **1**, 363 (1989).
[11] Y. Sone, T. Ohwada, and K. Aoki, Phys. Fluids A **1**, 1398 (1989).
[12] T. Ohwada, Y. Sone, and K. Aoki, Phys. Fluids A **1**, 1588 (1989).
[13] G. Bird, *Molecular Gas Dynamics and the Direct Simulation of Gas Flows* (Clarendon Press, Oxford, 1994).
[14] C. Cercignani and S. Cortese, J. Stat. Phys. **75**, 817 (1994).
[15] K. Aoki, H. Yoshida, T. Nakanishi and A. L. Garcia, Phys. Rev. E **68**, 016302 (2003).
[16] D. R. Emerson, X. J. Gu, S. K. Stefanov, S. Yuhong and R. W. Barber, Phys. Fluids **19**, 107105 (2007).
[17] M. Tij and A. Santos, J. Stat. Phys. **76**, 1399 (1994).
[18] M. M. Mansour, F. Baras, and A. L. Garcia, Physica A **240**, 255 (1997).
[19] F. J. Uribe and A. L. Garcia, Phys. Rev. E **60**, 4063 (1999).
[20] K. Aoki, S. Takata and T. Nakanishi, Phys. Rev. E **65**, 026315 (2002).
[21] B. John, X. J. Gu and D. R. Emerson, Numer. Heat Transfer, Part B **58**, 287 (2010).
[22] B. John, X. J. Gu and D. R. Emerson, Comput. Fluids **45**, 197 (2011).
[23] B. John, X. J. Gu, and D. R. Emerson, in *Proceedings of 3rd Micro and Nano Flows Conference, Greece, 22–24 August 2011* (Brunel University Research Archive, Brunel University, London, 2011).
[24] C. Cercignani, M. Lampis and S. Lorenzani, Phys. Fluids **16**, 3426 (2004).
[25] X. J. Gu, D. R. Emerson and G. H. Tang, Continuum Mech. Thermodyn. **21**, 345 (2009).
[26] T. Ohwada, Y. Sone and K. Aoki, Phys. Fluids A **1**, 2042 (1989).

[27] Y. Zheng, A. L. Garcia and B. J. Alder, J. Stat. Phys. **109**, 495 (2002).
[28] S. Varoutis, C. Day and F. Sharipov, Vacuum **86**, 1952 (2012).
[29] M. Wang and Z. Li, Int. J. Heat Fluid Flow **25**, 975 (2004).
[30] B. John and M. Damodaran, Int. J. Numer. Meth. Fluids **61**, 1273 (2009).
[31] M. Darbandi and E. Roohi, Int. Comm. Heat Mass Transf. **38**, 1443 (2011).
[32] B. John and M. Damodaran, IEEE Trans. Magn. **45**, 4929 (2009).
[33] B. John, Ph.D. thesis, Nanyang Technological University, 2009.
[34] F. J. Alexander, A. L. Garcia and B. Alder, Phys. Fluids **10**, 1540 (1998).
[35] N. G. Hadjiconstantinou, Phys. Fluids **12**, 2634 (2000).
[36] N. G. Hadjiconstantinou, A. L. Garcia, M. Z. Bazant, and G. He, J. Comput. Phys. **187**, 274 (2003).
[37] C. Cercignani, M. Lampis and S. Lorenzani, Phys. Fluids **16**, 3426 (2004).